Precision Engineering 43 (2016) 335–344

Contents lists available at ScienceDirect

Precision Engineering

journal homepage: www.elsevier.com/locate/precision

Using a high-stiffness burnishing tool for increased dimensional and geometrical accuracies of openings

Branko Tadic[a], Sasa Randjelovic[a], Petar Todorovic[a], Jelena Zivkovic[a], Vladimir Kocovic[a], Igor Budak[b], Djordje Vukelic[b,*]

[a] University of Kragujevac, Faculty of Engineering, Department for Production Engineering, 34000 Kragujevac, Serbia
[b] University of Novi Sad, Faculty of Technical Sciences, Department for Production Engineering, 21000 Novi Sad, Serbia

ARTICLE INFO

Article history:
Received 2 December 2014
Received in revised form 2 August 2015
Accepted 28 August 2015
Available online 3 September 2015

Keywords:
Ball burnishing
Dimensional accuracy
Geometrical accuracy
Openings

ABSTRACT

The paper investigates ball burnishing of openings. A special high-stiffness tool was designed for the purpose of experimentation, allowing the burnishing of 40–120 mm openings. Experiments were performed with aluminium alloy EN AW-6082 (AlMgSi1). The primary goal was to achieve dimensional and geometrical accuracy of the openings. Using a specially designed stiff tool, the openings were widened by 0.06 mm on average, while the roundness and cylindricity errors were drastically reduced, especially at greater ball penetration depths. In addition, the surface roughness was improved by 35%. FEM analysis was conducted to determine the stress field distribution in the workpiece, as well as to approximate the residual stresses after the ball burnishing. Considering the experimental results, further investigation should be directed towards the achievement of high dimensional and geometrical accuracies, as well as increased process productivity.

1. Introduction

To provide the best performance and required product lifetime, it is necessary to satisfy numerous prerequisites, such as dimensional accuracy, geometrical accuracy, and surface finish. The surface finish is vital to the functional characteristics of surfaces, such as wear resistance, corrosion resistance, fatigue strength and losses due to friction. The most popular machining technologies – precision turning, reaming, milling, and even grinding – cannot always satisfy the required high surface quality. An improvement of surface finish can be achieved by treatments such as honing, lapping, super finishing and burnishing [1,2].

Ball burnishing is a finishing process in which a ball is rolled over the workpiece surface, which results in Hertzian contact pressures. These contact pressures exceed that of the yield, which causes plastic deformation of the workpiece surface layer. A plastic flow of the surface roughness profile peaks takes place, thus filling the adjacent valleys. By this process, the rough surface texture is evened out and the surface becomes smoother. The described method also contributes to the formation of hard surface layers due to deformation strengthening. The workpiece surface layers that undergo plastic deformation acquire special characteristics, while, due to previous machining processes, the residual surface stresses become transformed into compression stresses. The penetration depth of these compression stresses and the thickness of the strengthened surface layer depend on the workpiece material and applied loads. The compression stresses decrease towards the centre of the workpiece, and the depth of penetration depends on the workpiece material and applied load [3,4].

The burnishing process can be applied to workpieces of various materials, such as steels [5–9], aluminium alloys [10–18], titanium alloys [19,20], magnesium–calcium alloys [21], and brass alloys [22,23]. Additionally, it is possible to burnish workpieces of various geometries.

Many investigations of burnishing processes were focused on the ball burnishing process, due to its advantages, such as flexibility, low price, simple machining, etc.

El-Axir [16] studied the relationships between the fatigue life, the residual stress, and the ball burnishing process parameters. The experimental work was focused on establishing the effect of burnishing parameters (burnishing speed, force, and feed) on the residual stress and fatigue life of aluminium alloy 6061-T6. The residual stress distribution in the surface region due to ball burnishing was determined using a deflection-etching technique. Bougharriou et al. [8] performed an analytical study and finite element (FE) modelling to provide a fundamental understanding of burnishing on an AISI 1042 workpiece. The simulations were devoted to the study of the surface profile, the residual stresses

* Corresponding author. Tel.: +381 21 485 23 26; fax: +381 21 454 495.
E-mail address: vukelic@uns.ac.rs (D. Vukelic).

http://dx.doi.org/10.1016/j.precisioneng.2015.08.014
0141-6359/

and the influence of the burnishing parameters (penetration depth, feed rates, diameter of the ball of burnishing tool and initial surface quality) on the surface roughness and the residual stress distribution. Mohammadi et al. [20] developed a FE model for the simulation of a low plasticity burnishing process. The FEA model was used to investigate the effect of the main parameters, including the ball diameter, burnishing force, burnishing feed, and number of passes on the resultant profile of the residual stress and plastic deformation. They used design of experiments combined with the response surface methodology to develop smooth response functions to efficiently and accurately approximate the residual stress profile and plastic deformation. Sayahi et al. [19] presented 2D and 3D finite element (FE) ball burnishing models. The FE analysis was based on the elastic-plastic model of the material. They discussed the capability of the proposed models to predict the residual stresses created by the process. The results show that the 3D FE model predicted the residual stresses and provided useful information regarding the effect of the process parameters.

Rao et al. [6] established the effects of ball burnishing parameters on the surface hardness of high-strength low-alloy steel dual-phase steel specimens. A statistical analysis showed that the speed, feed, lubricant and ball diameter had significant effects on the surface hardness. Abu Shreehah [23] evaluated the effect of different burnishing conditions on the surface micro hardness, surface roughness, and form accuracy. Optimum burnishing parameters were established that minimized roughness and/or maximized surface hardening. Empirical formulas were developed to predict the surface micro hardness and roughness of leaded brass obtained by burnishing. Basak and Goktas [17] discussed the effect the number of revolutions, feed, number of passes, and pressure force have on the surface roughness and surface hardness in Al 7075 T6 materials. A fuzzy logic model was used to predict the best parameters for the burnishing process. El-Taweel and El-Axir [22] applied the Taguchi technique to identify the effects of burnishing parameters – burnishing speed, burnishing feed, burnishing force and number of passes – on the surface roughness, surface micro-hardness, improvement ratio of surface roughness, and improvement ratio of the surface micro-hardness. An analysis of variance (ANOVA), the signal-to-noise (S/N) ratio and an additive model were used to analyze and evaluate the optimum combination of the levels of the ball burnishing process parameters. Esme [13] investigated the multi-response optimization of the burnishing process for an optimal parametric combination to yield favourable surface roughness and micro hardness using the Grey relational analysis and Taguchi method. The significance of the burnishing parameters regarding the quality characteristics of the burnishing process was evaluated with ANOVA. Babu et al. [7] evaluated the effects of various burnishing parameters on the surface characteristics, surface microstructure, micro hardness in the case of steels, aluminium alloy and alpha-beta brass. The Taguchi technique was employed in the investigation to identify the parameters that most affect the surface roughness.

Sai and Lebrun [24] analyzed the evolution of the residual stresses, micro hardness, and roughness in relation to the finishing process (turning, grinding, burnishing). Different results showed that burnishing creates good surface quality, which improves wear resistance, fatigue, tensile strength, and corrosion resistance. El-Tayeb et al. [15] designed tools with an interchangeable adapter for burnishing. Ball burnishing processes were performed on aluminium 6061 workpieces with different parameters and different burnishing orientations to investigate the role of the burnishing speed, burnishing force and burnishing tool dimensions on the surface qualities and tribological properties. Esme et al. [14] developed a surface roughness prediction model using an artificial neural network (ANN) to investigate the effects of burnishing conditions during machining of AA 7075. The ANN model of the surface roughness parameters was developed considering the burnishing force, number of passes, feed rate and speed. Ibrahim et al. [9] examined the use of a ball burnishing tool (follower rest) to achieve good surface characteristics, such as a higher surface finish and reduced out-of-roundness. The effects of three burnishing parameters – the burnishing speed, feed, and force – on the out-of-roundness were studied. The experimental results were used as a knowledge base to prepare a fuzzy logic model that controls the burnishing parameters. Tadic et al. [18] discusses the effects of the ball burnishing process with consideration of the initial surface roughness, i.e., the workpiece condition due to previous machining. The burnishing was performed using a specially designed tool of high stiffness. The authors assumed that, compared to its previous counterparts with coiled springs, a high-stiffness tool should increase the surface quality. Esme et al. [25] used regression and neural network techniques for predicting the surface roughness in the ball burnishing process. The effects of the main burnishing parameters on the surface roughness were determined. Gharbi et al. [10] developed a specially designed burnishing tool device for treating large flat surfaces. They also developed a mathematical model to predict the surface roughness as a function of the speed, force, and feed rate. The results showed that the burnishing of aluminium 1050A plates improved their ductility, but not their micro-hardness. Furthermore, the effect of the burnishing loads on the residual stresses was found to depend on the feed direction. Stalin and Vinayagam [5] applied response surface methodology for the optimization of the ball burnishing process of tungsten carbide and tool steel. The input parameters were the burnishing force, feed, speed and number of passes. The output parameters were the surface roughness and surface hardness. Sagbas [11] presented a strategy based on the desirability function approach together with response surface methodology to optimize the ball burnishing process of 7178 aluminium alloy. The burnishing force, number of passes, feed rate and speed were considered as model variables. The results indicated that the burnishing force and number of passes were the significant factors determining the surface roughness. Travieso-Rodriguez et al. [12] presented the results of tests performed with a burnishing process that was applied to workpieces with convex or concave surfaces of two different materials (aluminium A92017 and steel G10380). The results of measurements of the surface roughness before and after burnishing were compared.

Most of the previous ball burnishing investigations were focused on the residual stresses and surface hardness, as well as the effects of the process parameters – mainly the pressure, force, speed, feed rate, number of passes, ball diameter, and lubricant – on the surface integrity. Ball burnishing can be used for the internal and external treatment of cylindrical and flat surfaces. As previously discussed, burnishing can also be used to treat openings. However, there are very few reports of this type of experimentation, and they mostly pertain to roller burnishing [26–30]. A small number of studies relate to the ball burnishing of openings [31,32]. El-Axir et al. [31] used response surface methodology to improve the experimentation design without a loss of accuracy of the results. Mathematical models were presented for predicting five different surface profile parameters caused by the internal ball burnishing process parameters, namely, the burnishing speed, feed, depth of penetration, and number of passes. El-Axir et al. [32] designed a simple ball burnishing tool for inner surface processing. They established the effect of the burnishing parameters on the roundness and surface micro hardness of aluminium alloy workpieces.

In contrast to previous investigations, the focus in this paper is placed on achieving the desired dimensional and geometrical accuracies of openings using a ball burnishing process with a highly stiff tool.

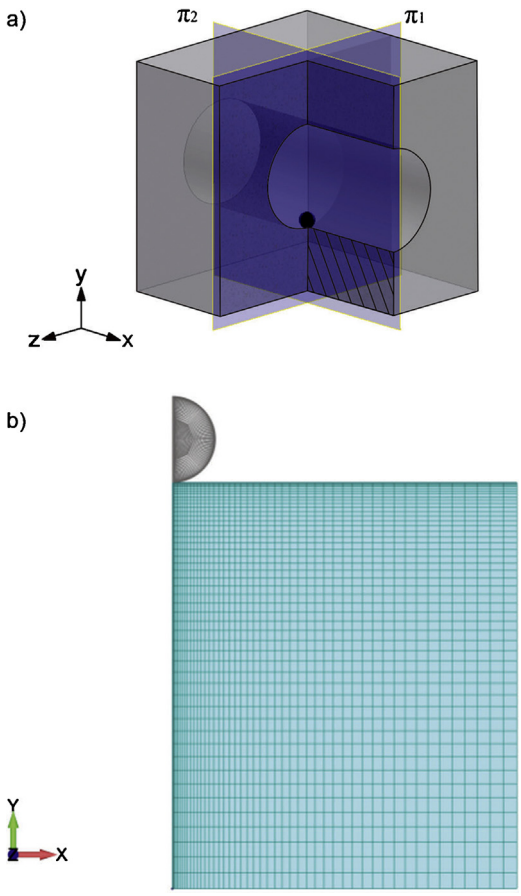

Fig. 1. The model used in the FEM analysis: (a) 3D rendering, and (b) finite elements mesh.

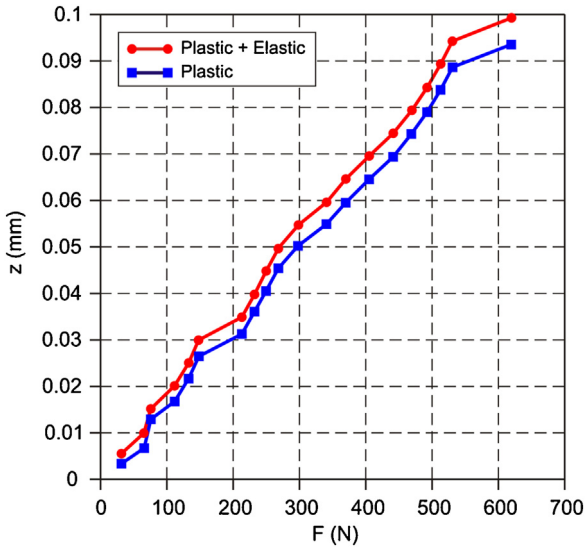

Fig. 2. Dependence between the penetration force and ball penetration depth along the *y*-axis. (For interpretation of the references to colour in text near the reference citation, the reader is referred to the web version of this article.)

2. Theoretical background

FEM analysis was used for the analytical analysis of the ball burnishing process. Software for non-linear analysis, Femap with the PAK-S solver, was used [33]. The goal of the numerical experiments was to determine the stress field distribution within the workpiece, as well as to approximate the residual stresses in the finished part due to the ball burnishing process. In addition, it was very important to establish the fraction of elastic deformation in the total deformation. That was crucial, considering the previously established goal to achieve dimensional accuracy of the opening by ball burnishing.

The model (Fig. 1a) used for the simulation of the ball burnishing process consists of two elements: the workpiece and the burnishing ball with a 7 mm diameter, which penetrates the workpiece. The workpiece was modelled as a box with an opening (Fig. 1a). The cross-section between the workpiece and plane π_1, which is perpendicular to the opening axis of symmetry, was considered. The resulting cross-section was then considered as an axisymmetrical model in which the axis of symmetry, i.e., plane π_2 (Fig. 1a), runs through the centre of the burnishing ball. This simplification was introduced to reduce the total analysis time. Boundary conditions were set such that the displacements were zero on the axis of symmetry in the direction perpendicular to the axis. To simulate the workpiece support, the displacements of the lower workpiece surface in the direction of *y*-axis were set to zero.

The workpiece was meshed with 4500 4-node finite elements, resulting in a total of 4672 nodes (Fig. 1b). It is important to note that the mesh was refined in the contact zone. The edge lengths of the finite elements within the modelled contact zone were 22 μm and 26 μm, respectively. 2D FEM analysis was conducted with the depth of the ball penetration varying from 0 to 0.1 mm with an increment of 5 μm. A total of 20 numerical experiments were performed.

It is important to note that the model does not allow a complete simulation of the ball burnishing process because the modelled ball did not perform the rolling on the workpiece surface. Instead, the numerical experiments simulated only ball penetration to the desired depth, after which the workpiece was unloaded. However, the model allowed the authors to approximate the reaction forces due to the ball penetration and to establish the stress field distribution within the workpiece during burnishing, as well as the residual stresses that remained after unloading. Furthermore, the fraction of elastic deformation was also established, which was crucial from the aspect of dimensional accuracy of the burnished opening.

Based on the results obtained through 20 numerical experiments, a curve was plotted that defines the relationship between the penetration force and penetration depth. Shown in Fig. 2 are two curves: the red one represents the displacement of the node in contact with the ball, and the blue curve represents the actual displacement of the node after the unloading.

One can notice from Fig. 2 that once the workpiece is unloaded, an elastic recovery of the considered node takes place. It is very important to establish the fraction of elastic deformation because that allows the real node displacement after the unloading to be determined. As previously stated, this information is essential for the achievement of dimensional and geometric accuracies. It was determined that the increase of the elastic recovery effect is directly proportional to the ball penetration depth.

Shown in Fig. 3 is the development of the stress fields at 50% and 100% of the burnishing process for the selected ball penetration depth of 30 μm. The stress fields distribution and their evolution during ball penetration into the workpiece are easily noticed. At the end of penetration, the maximum stress is reached and is approximately 70 MPa directly under the treated surface, i.e., in nodes located at the upper workpiece surface.

Fig. 4 illustrates the stress distribution in the workpiece after unloading, for the same case of a 30-μm ball penetration depth. The stress fields show residual stress within the workpiece. The maximum stress after unloading is, interestingly, approximately equal

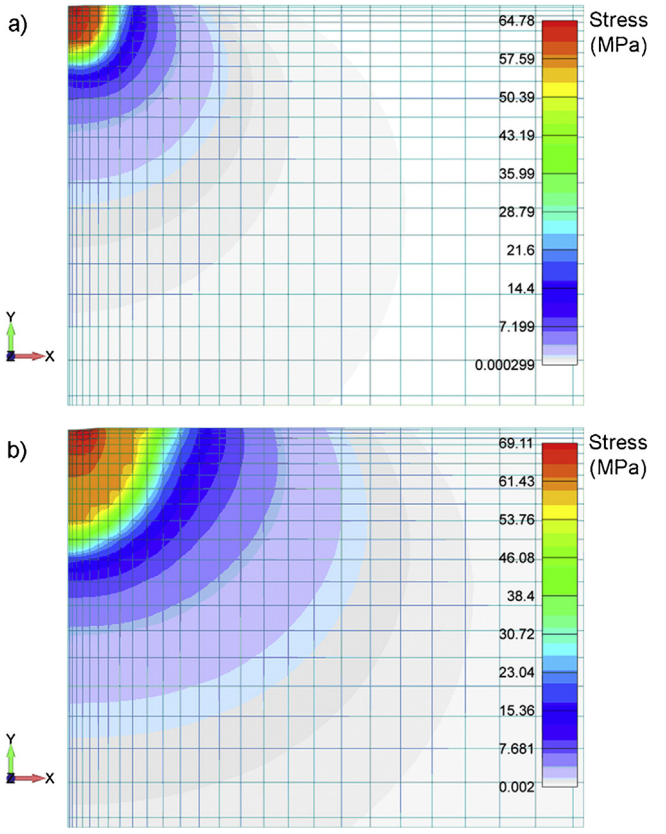

Fig. 3. Evolution of the stress fields distribution during ball penetration at the depth of 30 μm at process completion of (a) 50% and (b) 100%.

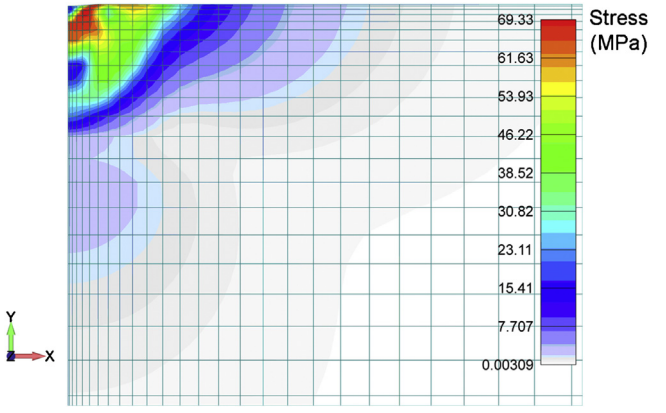

Fig. 4. Stress fields distribution in the workpiece for a 30 μm ball penetration depth and subsequent unloading.

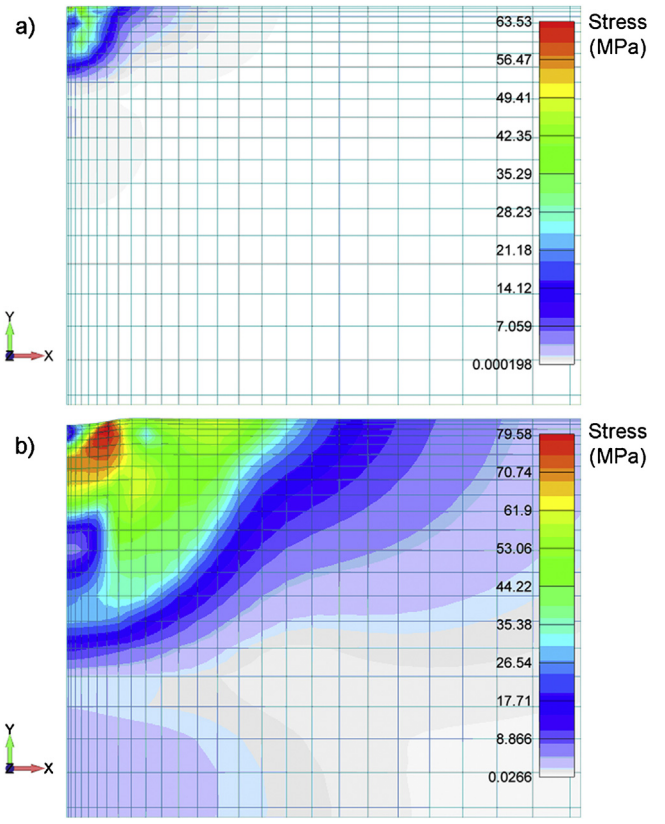

Fig. 5. Stress fields distribution in the workpiece after unloading, obtained for ball penetration depths of (a) 10 μm and (b) 100 μm.

Table 1
Chemical composition.

Element	Si	Fe	Mn	Mg	Cr	Zn	Ti	Al
wt. %	0.9	0.5	0.6	0.9	0.25	0.2	0.1	Balance

Table 2
Physical properties.

Specific weight G (g/cm^3)	2.7
Modulus of elasticity E (GPa)	69
Yield strength $R_{p0.2}$ (N/mm^2)	240–255
Tensile strength R_m (N/mm^2)	275–300
Hardness (HB)	89
Lin. coef. of thermal expan. (20–100 °C) α (μm/m °C)	23.4
Thermal conductivity κ (W/mK)	165–185

to the stress achieved at 100% of penetration, with the important difference that the location of the maximum stress after unloading is offset towards the internal section of the workpiece, no longer being directly beneath the workpiece surface. This offset can be explained by the very effect of elastic recovery of the surface nodes.

Shown in Fig. 5 is a comparative depiction of the stress fields distribution within the workpiece for the various depth penetrations after unloading. It can be noted from Fig. 5 that the stress after unloading increases with increasing ball penetration depth. Thus, a 10-μm penetration depth results in a maximum stress of approximately 63 MPa, whereas at a 100-μm penetration depth, the maximum stress reaches 80 MPa.

3. Experimental investigation

Experiments were conducted on a 120 × 120 × 56 mm workpiece made of aluminium alloy EN AW-6082 (AlMgSi1). The chemical composition of the workpiece is shown in Table 1, and its physical properties are listed in Table 2.

The plan of experiment is shown in Fig. 6. First, seven stepped openings are machined on the workpiece by planetary milling, using a Haas TM-1 milling machine. The depth of each opening is 8 mm. The diameter of each successive opening decreases incrementally by 10 μm. The starting diameter, i.e., the diameter of the largest opening, equals 54.0020 mm, leading incrementally to the smallest opening of 53.9320 mm. This initial machining allowed subsequent ball burnishing with six theoretical penetration depths, incremented by 5 μm (z = 5, 10, 15, 20, 25, 30 μm), which produced six different surfaces. Furthermore, it is important to note that the first and largest opening (54.0020 mm) was used to adjust the

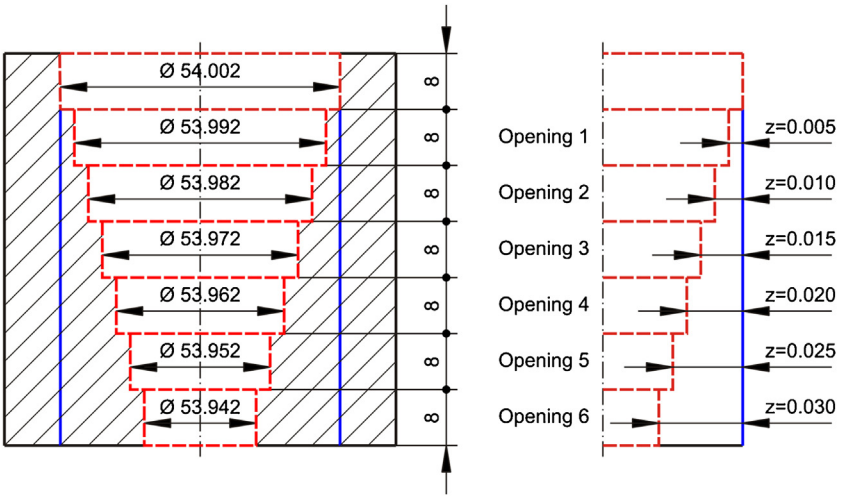

Fig. 6. Plan of experiment. (For interpretation of the references to colour in text near the reference citation, the reader is referred to the web version of this article.)

burnishing tool to the required diameter, which in practice means that the three burnishing balls should be brought into contact with the surface of the required opening. The penetration depth for the first opening was zero, meaning that the first opening was not ball burnished.

The processing of the openings using a specially designed stiff burnishing tool is performed over the length of 48 mm. The first opening is not burnished, while the remaining six milled openings (the blue line in Fig. 6) are subjected to ball burnishing. The diameter of the burnishing balls used in this experiment was 7 mm. Burnishing was performed on a Haas TM-1 CNC milling machine, at $n = 200$ rpm and a feed rate of $f = 50$ mm/min. The processing regime was selected to avoid the superposition of ball trajectory paths, meaning that the burnishing was performed in one pass. Photographs of the burnishing tool mounted on the milling machine and during processing are shown in Fig. 7.

A detailed model of the burnishing tool specially designed for this experiment is shown in Fig. 8. The tool was designed with the following requirements in mind: to eliminate the error of the machine tool spindle assembly, to allow processing of a wider range (40–120 mm) of diameters with one tool, to achieve dimensional accuracy and improve the surface quality of the openings, as well as some other physical and chemical properties which are omitted from consideration in this paper (wear resistance and corrosion, increased surface hardness, etc.), and finally, to allow acceptable costs and processing time.

Functionally, the tool assembly can be broken down into four modules: the tool carrier (flange) (position 1), the base plate with openings to allow mounting of the bearing support (position 2), the ball bearing support (position 3) and the threaded nut (position 4). The tool carrier (position 1) has a holder (position 1a) mounted onto the machine tool spindle assembly by a Ø20 mm collet. There is a groove on the tool carrier (position 1b) that allows the mounting of two short axles (position 5), which provide the connection to the base plate (position 2). Such design solution was chosen to allow the adjustment of the tool to the diameter of the opening being processed, which, in turn, reduces the spindle assembly error of the host machine tool. Bearing in mind the wide range of opening diameters (40–120 mm), three different base plates were designed (position 2) with openings to allow connection to the bearing supports (position 3). A particular base plate is selected depending on the diameter of the processed opening. The role of the ball bearing support (position 3) is to accommodate the burnishing ball (position 6) and to allow it to roll smoothly while avoiding skidding over the workpiece surface. Smooth rolling is achieved by the three

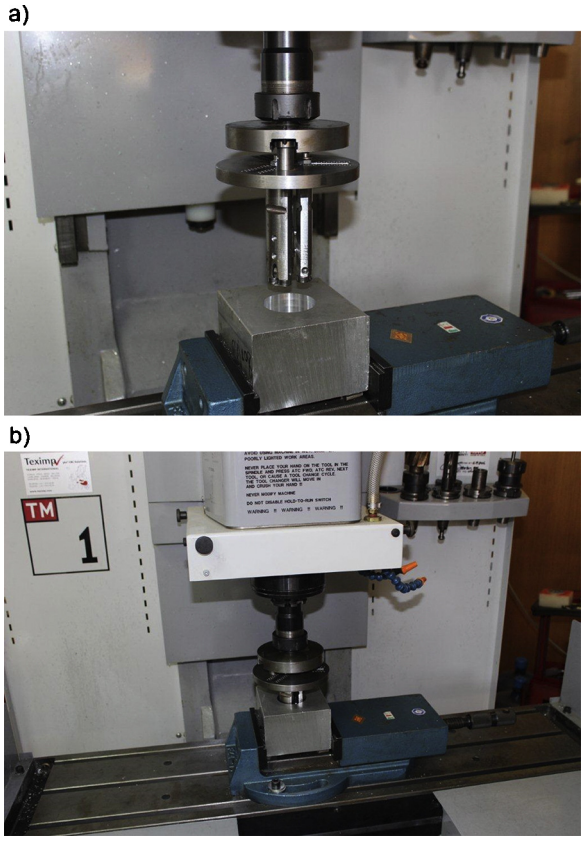

Fig. 7. Ball burnishing tool used in the experiment (a) mounted on the milling machine, and (b) during the process.

roller bearings (position 7). Three bearing supports are mounted onto the base plate at an angle of 120° relative to each other. Once the ball holders (position 8) are fastened to the ball bearing support (position 3) by special screws (position 9), the balls fit into the openings "H" which are positioned on the ball holders. Due to the clearance present between the bearings (position 7) and the balls, prior to surface treatment, the balls are pressing against the opening "H" and are not in contact with the roller bearings. During the surface treatment, due to the burnishing forces, each ball is detached from the ball holder – plate – (position 8) and establishes contact with the three roller bearings. During the surface treatment,

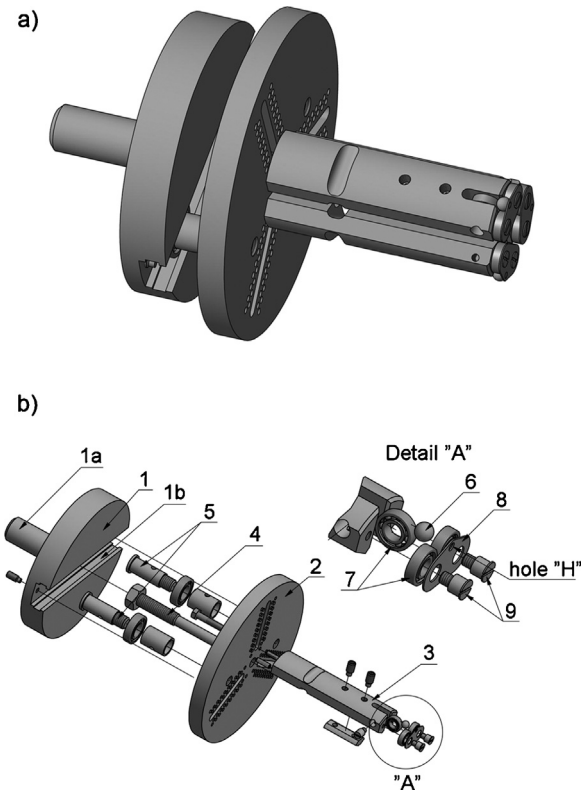

Fig. 8. Ball burnishing tool, (a) CAD model, and (b) exploded view.

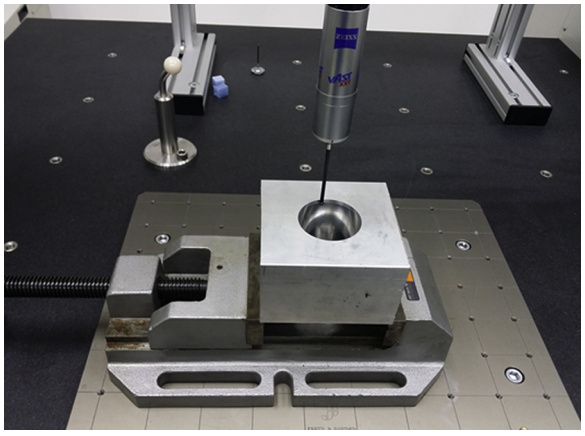

Fig. 9. Measurement process.

there is no physical contact between the balls and the ball holders. The bearing supports can accommodate burnishing balls of various diameters. A specially designed nut (position 4) has at its free end a 10° cone. Turning the nut increases the load on the bearing support, thus directly adjusting the deflection at the free end of the bearing support. A single full turn of the nut results in a 0.1 mm displacement at the free end of the support bearing. This is of utmost importance because it provides the penetration of the burnishing ball into workpiece surface. Such design solution provides a stiff tool-ball-workpiece system for openings.

4. Results

Characteristic openings were measured before and after burnishing on a Carl Zeiss Contura G2 coordinate measuring machine with 0.0001 mm accuracy (Fig. 9). The measurements were conducted in controlled micro-climatic conditions (temperature 20.0 ± 0.5 °C, humidity 50 ± 2%). A straight styli measurement probe was used (length, $L = 75$ mm, probe tip diameter, $R = 2.5$ mm).

A scanning strategy was used to conduct measurements. The scanning speed was 25 mm/s, while the increment for point acquisition was 0.5 mm, and thus, to span the 8 mm height of each scanned opening, 16 measurements were performed in each opening.

Shown in Table 3 are the measurement results for all the opening diameters ($D_{\text{mill.}}$) after milling (prior to ball burnishing) and after the ball burnishing operation ($D_{\text{bur.}}$). In both cases, the mean diameter values are given and were obtained using the previously described scanning strategy. Based on the data in Table 3, it can be concluded that there is a difference of the opening diameters prior to and after the burnishing operation. It is also worth noting that higher ball penetration depths yield smaller deviations of the mean diameter ($D_{\text{bur.}}$) compared to the nominal diameter ($D_{\text{nom.}}$), which for all openings equals 54.0020 mm. The largest deviation is measured on opening 1 and equals 0.0088 mm, whereas opening 6 has the smallest deviation of 0.0012 mm.

Table 4 shows the calculated values for the theoretical, required and actual depth of the ball penetration into the workpiece material. The theoretical penetration depth is one half of the difference between the theoretical diameters as per the engineering drawing (Fig. 6). The required penetration depth is one half of the difference between the theoretical diameter after ball burnishing (54.0020 mm according to Fig. 6 for all openings) and the diameter of the opening before ball burnishing. The actual penetration depth is one half of the difference between the mean opening diameter after and prior to ball burnishing. Considering the results from Table 4, one concludes that there is a certain difference between the theoretical, required, and actual penetration depths. The actual ball penetration depth for each opening is higher than the theoretical depth; however, it is also lower than the required penetration depth that would result in the theoretical opening diameter after ball burnishing, which is 54.0020 mm for all openings.

Table 3
The results of measurements of opening diameters.

Opening	Diameter			Deviation
	$D_{\text{nom.}}$ (mm)	$D_{\text{mill.}}$ (mm)	$D_{\text{bur.}}$ (mm)	$\lvert D_{\text{nom.}} - D_{\text{bur.}} \rvert$ (mm)
1	54.0020	53.9999	54.0108	0.0088
2	54.0020	53.9789	53.9998	0.0022
3	54.0020	53.9688	53.9993	0.0027
4	54.0020	53.9599	54.0001	0.0019
5	54.0020	53.9412	54.0005	0.0015
6	54.0020	53.9357	54.0008	0.0012

Table 4
Theoretical, required and actual ball penetration depths.

Opening	Penetration depth z (mm)		
	Theoretical	Required	Actual
1	0.005	0.0011	0.0055
2	0.010	0.0115	0.0104
3	0.015	0.0166	0.0152
4	0.020	0.0211	0.0201
5	0.025	0.0304	0.0297
6	0.030	0.0332	0.0326

Table 5
Results of the cylindricity measurements.

Opening	1	2	3	4	5	6
Cylindricity (mm)	0.0317	0.0198	0.0173	0.0163	0.0155	0.0149

Table 6
Results of the roundness measurements.

Opening	1	2	3	4	5	6
Roundness (mm)	0.0088	0.0022	0.0027	0.0019	0.0015	0.0012

Table 7
Ra values for openings 1–6.

Opening	1	2	3	4	5	6
Ra (μm)	0.600	0.560	0.535	0.576	0.603	0.629

Shown in Table 5 are the results of measurements of the opening cylindricity. The maximal deviation from cylindricity was detected in opening 1 and equals 0.0317 mm. The minimal deviation from cylindricity was detected in opening 6 and equals 0.0149 mm. The mean deviation from cylindricity equals 0.0193 mm.

Shown in Table 6 are the results of the roundness measurements. The maximal deviation of 0.0088 mm from roundness was again detected in opening 1. Opening 6 had the minimal deviation from roundness of 0.0012 mm. The mean deviation from roundness is 0.0031 mm.

Plots of the roundness deviations are shown in Fig. 10. The red circles denote the maximal and minimal diameter measurements. The black circle denotes the mean diameter value. The green and orange areas represent the positive and negative deviations from the mean diameter. It is seen from Fig. 10 that opening 1 has the maximal deviation.

The surface roughness measurements were performed using a Rank Taylor Hobson Talysurf 6 profiler with a variable-inductance transducer and a 2 μm stylus tip. The reference measuring length of the profile was 1.25 mm.

The initial surface roughness before burnishing was measured on all of the six openings. Measurements were taken on every opening along the three equidistant lines parallel to the central axis. A total of 18 measurements were taken. The minimum initial surface roughness was $Ra_{min} = 0.729$ μm, whereas the maximum was $Ra_{max} = 0.869$ μm. The arithmetic mean value of the initial surface roughness was $\overline{Ra} = 0.818$ μm.

Shown in Table 7 are the results of the Ra measurements after ball burnishing.

Fig. 11a shows the change in the roughness profile (Ra) for the six openings after the ball burnishing. Judging by the roughness values from Fig. 11a, it is noted that the lowest surface roughness after the ball burnishing was detected in opening 3 and equals Ra = 0.535 μm. Also worth noting is the fact that the surface roughness diminishes with increasing depth penetration up to a certain value, after which the roughness slightly increases. After the ball burnishing, opening 6, which features the largest ball penetration depth, has the largest surface roughness of Ra = 0.629 μm.

Shown in Fig. 11b are the surface roughness profiles of opening 3, which had the lowest surface roughness of all the openings both before and after the burnishing process.

5. Discussion

Based on a review of the available investigations on the topic of ball burnishing, it was concluded that the tool stiffness plays a key role in achieving geometrical accuracy and adequate surface quality. With that in mind, a very stiff and adaptable tool was designed for the processing of openings by ball burnishing. The tool provides free rolling of the three balls over the workpiece surface without skidding, which is crucial for achieving the optimal surface roughness. Due to its ability to adjust to the opening diameter, the tool can be used on machine tools (in this case, a milling machine) that feature a certain spindle assembly error.

Considering the results from Tables 3 and 4, it is notable that the change of opening diameter after ball burnishing corresponds to the ball penetration depth. More precisely, there is a certain deviation between the required and actual value of the opening diameter. It is evident that the difference between the required and actual values of the opening diameter decreases with an increasing ball penetration depth. The difference can be attributed to elastic deformations of the workpiece on the one side and the tool on the other – and above all, to the elastic deformations of the ball bearing. This problem can be eliminated by an increased stiffness of the tool design. All this leads to the conclusion that ball burnishing by a high-stiffness tool can provide dimensional accuracy, which is highly important in many machining processes (e.g., machining of large-diameter openings to accommodate ball bearings).

Because there is a deviation between the actual and required values of the opening diameter, an FEM analysis was conducted to establish the fraction of the elastic workpiece deformation in the total deformation. The discussed 2D FEM model allowed the presence of elastic workpiece deformations to be determined, as shown in Fig. 2. Furthermore, the proposed 2D FEM model also allowed the workpiece stresses to be determined during the ball penetration, as well as after the unloading. As expected, the stress increases with the ball penetration depth.

The results of the FEM analysis show that the increase of the elastic recovery effect is directly proportional to the ball penetration depth. On the other hand, the results of the experimental investigation (Table 4) reveal that with increasing penetration depth, the depth of the elastic recovery first decreases and then increases. The present deviations between the simulation and experimental results can be attributed to the influence of the workpiece clamping forces as well as the heat generated during ball burnishing.

Workpiece clamping (Fig. 7) was applied within the zones of openings 5 and 6. It is precisely in these zones (Table 4) that the maximum deviations between the theoretical and actual penetration depths were observed. In the zone of opening 5, these deviations equal 4.7 μm, while they are 2.6 μm in the zone of opening 6. Reductions of the opening diameters in zones 5 and 6 prior to ball burnishing are due to the clamping forces. Thus, due to the diameter reduction in the zones of openings 5 and 6, the depth of penetration exceeded the theoretical and required values. However, this was not the case with the other openings (1–4).

In addition, the ball burnishing process is accompanied by certain temperature effects. During rolling, the burnishing balls generate heat, which causes the workpiece material to expand. This also affects the opening diameters. Regardless of the fact that the balls generate a smaller amount of heat during rolling, the impact of the temperature gradient on the penetration depth can be significant, especially considering the following issues:

- The linear coefficient of thermal expansion (20–100 °C) is $\alpha = 23.4$ μm/m °C, which cannot be neglected.
- Within the zones of openings 5 and 6, the workpiece is in contact with fixture elements that generate stresses on the workpiece contact surfaces. These stresses counteract the thermal stresses, keeping the thermal expansion of openings 5 and 6 in check. Consequently, the diameters of openings 5 and 6 contract in comparison to the other openings (openings 1–4), and thus contribute to a penetration depth that is larger than the nominal/theoretical value.

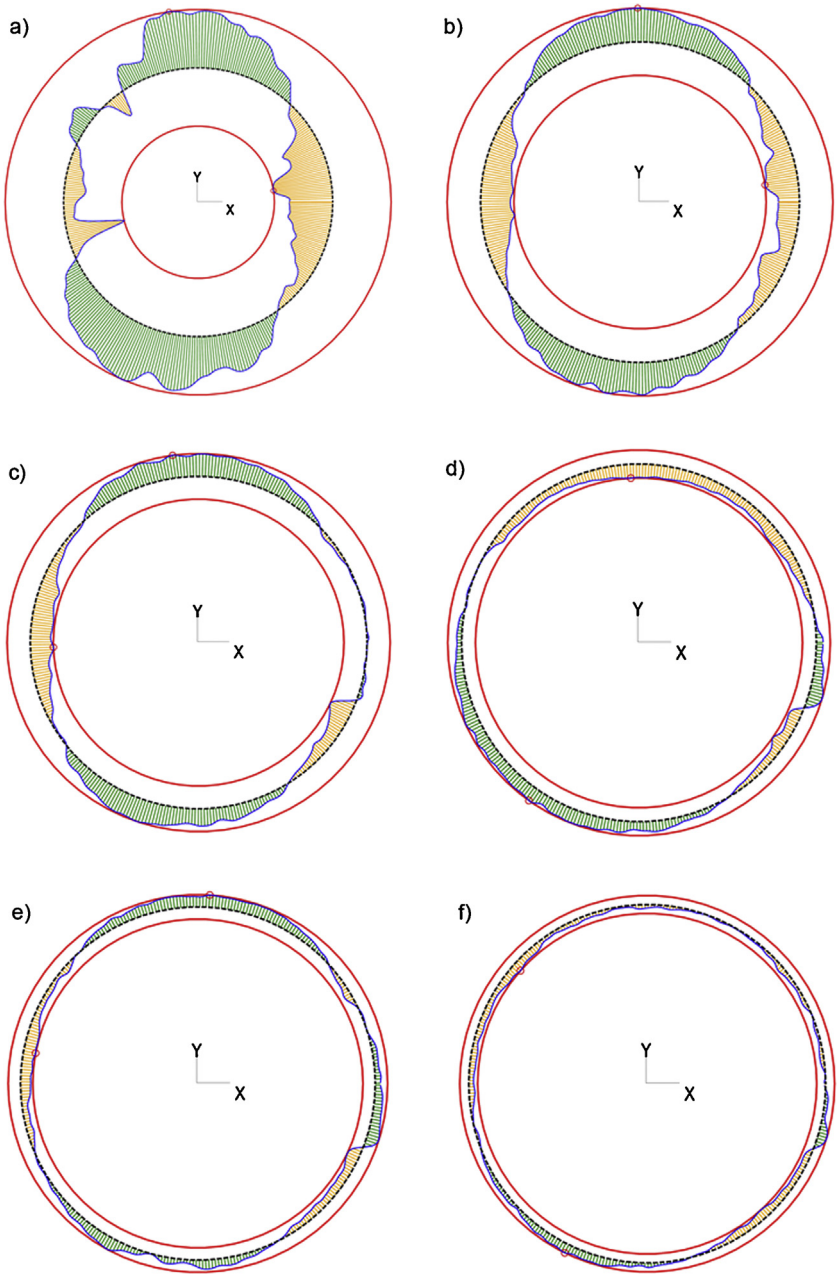

Fig. 10. Plots of the roundness deviations, (a) opening 1, (b) opening 2, (c) opening 3, (d) opening 4, (e) opening 5, (f) opening 6. (For interpretation of the references to colour in text near the reference citation, the reader is referred to the web version of this article.)

It should be noted that the discussed deviations are small, in the range of 0.0004–0.0047 mm.

In reference [18], a theoretical and experimental study on the influence of tool stiffness on the workpiece surface quality was presented. It was established that higher stiffness burnishing tools contribute to higher surface quality. The focus in this paper is placed on achieving the desired dimensional and geometrical accuracies of openings using a ball burnishing process. That means the required opening should have a tight tolerance. The burnishing tool consists of several parts. During the burnishing process, it sustains forces/resistances that load the tool via the balls. Theoretically, the mechanical model of the burnishing tool can be depicted as in Fig. 12.

The larger circle in Fig. 12 (with diameter d_1) marks the location of the balls prior to beginning the process. Due to resistive forces during the burnishing process (forces F_n and F_t), the balls assume the position marked with a smaller circle (with diameter d in Fig. 12). In other words, each ball has a radial displacement, which is denoted by z. The ball displacement in the tangential direction is not shown in the drawing because it is substantially smaller than the radial displacement and does not have a significant effect on the displacement z. The discussed displacement (z) occurs primarily due to elastic deformations within the ball/ball bearings contact interface and elastic deformations of the ball bearing support (position 3 in Fig. 8).

The burnishing tool assembly, ball bearings, ball bearing supports and other elements were designed to minimize the value of z by increasing their stiffness. This was necessary to achieve the required diameter of the openings within tight tolerances. The value of z was derived from the FEM analysis in the Femap software. The displacement z was calculated at the normal ball load of 200 N, which corresponds to a penetration depth of 0.030 mm,

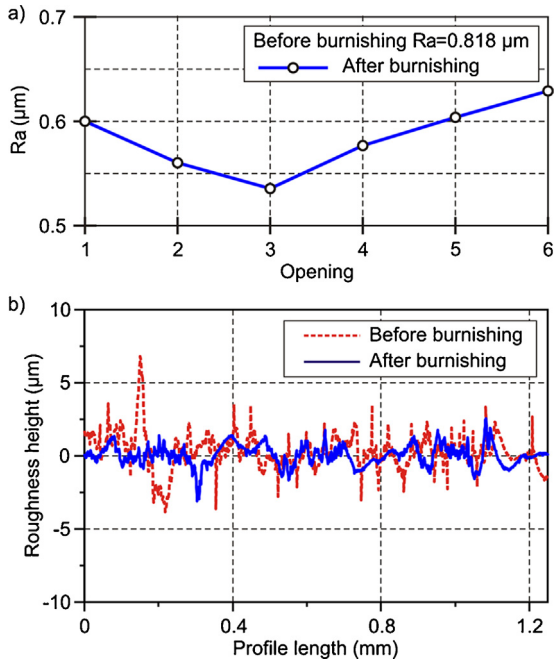

Fig. 11. Roughness, (a) diagram of the Ra variation for openings 1–6 and (b) the overlapped surface roughness profile before burnishing and roughness profile of opening 3 after ball burnishing.

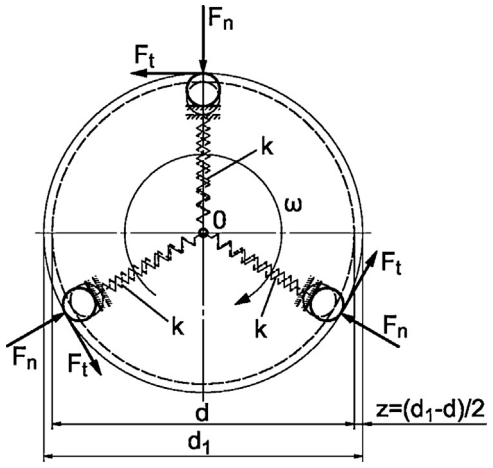

Fig. 12. Simplified mechanical model of ball burnishing of openings.

as seen in the Fig. 2. Based on the FEM analysis results the radial ball displacement is 0.00117 mm (1.17 μm), and this value can be used to calculate the burnishing tool stiffness as well as the force/displacement ratio:

$$k = F_n/z = 200/1.17 = 170.94\,(\mathrm{N/\mu m})$$

By analysing the data from Tables 5 and 6, one can conclude that ball burnishing with a high-stiffness tool does not affect the cylindricity and roundness errors. Moreover, compared to the value before the ball burnishing, which equalled 0.0056 mm, the mean roundness error decreased to 0.0031 mm. Similarly, compared to the value of 0.0440 mm before the ball burnishing, the mean cylindricity error dropped to 0.0193 mm. Also worth noting is that the cylindricity and roundness errors decrease with increasing ball penetration depth.

The data from Table 7 and Fig. 11a lead to the conclusion that the surface roughness is improved with increasing ball penetration depth up to some degree, after which the roughness begins to deteriorate.

Based on this, it can be concluded that the optimization of the ball penetration depth should be addressed to further improve the surface roughness and dimensional accuracy.

6. Conclusions

The use of high-stiffness tools enables better workpiece dimensional and geometrical accuracies. An analysis of the results allows one to conclude that it is possible to efficiently improve the dimensional and geometrical accuracies of milled openings using a specially designed tool. This ball burnishing tool allowed widening of the openings by a mean value of 0.06 mm, which is a significant result.

In addition to achieving the required opening diameter, it is highly important to emphasize that the cylindricity and roundness do not deteriorate but are instead improved with increasing ball penetration depth. A significant reduction of the cylindricity and roundness errors were detected after ball burnishing. The average reduction factor of the cylindricity error was 2.28, while the roundness error was reduced by a factor of 1.81.

In addition, the proposed burnishing method improved the surface roughness in all the openings. The initial surface roughness was improved on average by 35%. It should be noted that the arithmetic mean value of the initial surface roughness of $\bar{Ra} = 0.818$ μm corresponds to fine turning, i.e., milling. Based on previous investigations, the surface roughness can be improved even more than 35% in cases of rough initial machining; however, due to the adopted plan of experiment, the initial surface roughness in this experiment needed to be finer. Finally, the results of this investigation lead to the conclusion that it is also possible to optimize the ball penetration depth of the ball burnishing process to improve the workpiece surface roughness.

The authors maintain that future investigations should be directed towards achieving higher dimensional and geometrical accuracies, as well as the productivity of the ball burnishing process.

References

[1] Mahajan D, Tajane R. A review on ball burnishing process. Int J Sci Res Publ 2013;3:1–8.
[2] Todorovic P, Vukelic D, Tadic B, Veljkovic D, Budak I, Macuzic I, et al. Modelling of dynamic compliance of fixture/workpiece interface. Int J Simul Model 2014;13:54–65.
[3] Balland P, Tabourot L, Degre F, Moreau V. Mechanics of the burnishing process. Precis Eng 2013;37:129–34.
[4] Revankar DG, Shetty R, Shrikantha S, Rao SS, Gaitonde NV. Analysis of surface roughness and hardness in ball burnishing of titanium alloy. Measurement 2014;58:256–68.
[5] Stalin MRJ, Vinayagam BK. Optimization of ball burnishing process on tool steel (T215Cr12) in CNC machining centre using response surface methodology. Arab J Sci Eng 2011;36:1407–22.
[6] Rao DS, Hebbar HS, Komaraiah M. Surface hardening of high-strength low alloy steels (HSLA) dual-phase steels by ball burnishing using factorial design. Mater Manuf Processes 2007;22:825–9.
[7] Babu PR, Ankamma K, Prasad TS, Raj AVS, Prasad NE. Optimization of burnishing parameters and determination of select surface characteristics in engineering materials. Sadhana Acad Proc Eng Sci 2012;37:503–20.
[8] Bougharriou A, Sai WB, Sai K. Prediction of surface characteristics obtained by burnishing. Int J Adv Manuf Technol 2010;51:205–15.
[9] Ibrahim AA, Abd Rabbo SM, El-Axir MH, Ebied AA. Center rest balls burnishing parameters adaptation of steel components using fuzzy logic. J Mater Process Technol 2009;209:2428–35.
[10] Gharbi F, Sghaier S, Hamdi H, Benameur T. Ductility improvement of aluminum 1050A rolled sheet by a newly designed ball burnishing tool device. Int J Adv Manuf Technol 2012;60:87–99.
[11] Sagbas A. Analysis and optimization of surface roughness in the ball burnishing process using response surface methodology and desirability function. Adv Eng Softw 2011;42:992–8.
[12] Travieso-Rodriguez JA, Dessein G, Gonzalez-Rojas HA. Improving the surface finish of concave and convex surfaces using a ball burnishing process. Mater Manuf Processes 2011;26:1494–502.

[13] Esme U. Use of grey based Taguchi method in ball burnishing process for the optimization of surface roughness and micro hardness of AA 7075 aluminum alloy. Mater Tehnol 2010;44:129–35.
[14] Esme U, Sagbas A, Kahraman F, Kulekci MK. Use of artificial neural networks in ball burnishing process for the prediction of surface roughness of AA 7075 aluminum alloy. Mater Tehnol 2008;42:215–9.
[15] El-Tayeb NSM, Low KO, Brevern PV. Enhancement of surface quality and tribological properties using ball burnishing process. Mach Sci Technol 2008;12:234–48.
[16] El-Axir MH. An investigation into the ball burnishing of aluminium alloy 6061-T6. Proc Inst Mech Eng B: J Eng Manuf 2007;221:1733–42.
[17] Basak H, Goktas HH. Burnishing process on Al-alloy and optimization of surface roughness and surface hardness by fuzzy logic. Mater Des 2009;30:1275–81.
[18] Tadic B, Todorovic MP, Luzanin O, Miljanic D, Jeremic MB, Bogdanovic B, et al. Using specially designed high-stiffness burnishing tool to achieve high-quality surface finish. Int J Adv Manuf Technol 2013;67:601–11.
[19] Sayahi M, Sghaier S, Belhadjsalah H. Finite element analysis of ball burnishing process: comparisons between numerical results and experiments. Int J Adv Manuf Technol 2013;67:1665–73.
[20] Mohammadi F, Sedaghati R, Bonakdar A. Finite element analysis and design optimization of low plasticity burnishing process. Int J Adv Manuf Technol 2014;70:1337–54.
[21] Salahshoor M, Guo YB. Process mechanics in ball burnishing biomedical magnesium–calcium alloy. Int J Adv Manuf Technol 2013;64:133–44.
[22] El-Taweel TA, El-Axir MH. Analysis and optimization of the ball burnishing process through the Taguchi technique. Int J Adv Manuf Technol 2009;41:301–10.
[23] Abu Shreehah TA. Developing and investigating of elastic ball burnishing tool. Int J Adv Manuf Technol 2008;36:270–9.
[24] Sai WB, Lebrun JL. Influence of finishing by burnishing on surface characteristics. J Mater Eng Perform 2003;12:37–40.
[25] Esme U, Kulekci MK, Ozgun S, Kazancoglu Y. Predictive modelling of ball burnishing process using regression analysis and neural network. Mater Test 2013;55:187–92.
[26] El-Tayeb NSM, Low KO, Brevern PV. The influence of roller burnishing process on hardness and roughness of cylindrical polymer surfaces. Proc Inst Mech Eng J: J Eng Tribol 2008;222:947–55.
[27] Akkurt A. Comparison of roller burnishing method with other hole surface finishing processes applied on AISI 304 austenitic stainless steel. J Mater Eng Perform 2011;20:960–8.
[28] Akkurt A. Comparison of roller burnishing and other methods of finishing treatment of the surface of openings in parts from tool steel D3 for cold forming. Met Sci Heat Treat 2011;53:145–50.
[29] Ovali I, Akkurt A. Comparison of burnishing process with other methods of hole surface finishing processes applied on brass materials. Mater Manuf Processes 2011;26:1064–72.
[30] Akkurt A, Kurt A, Ozdemir A, Seker U. Comparison of hole surface finishing processes with roller burnishing method applied in copper materials. Gazi Univ J Sci 2014;27:721–34.
[31] El-Axir MH, Othman OM, Abodiena AM. Study on the inner surface finishing of aluminum alloy 2014 by ball burnishing process. J Mater Process Technol 2008;196:120–8.
[32] El-Axir MH, Othman OM, Abodiena AM. Improvements in out-of-roundness and micro hardness of inner surfaces by internal ball burnishing process. J Mater Process Technol 2008;202:435–42.
[33] Zivkovic M, Kojic M, Slavkovic R, Grujovic N. PAK-S program for FEM structural analysis. Kragujevac: Faculty of Mechanical Engineering; 2003.